JCBI
Journal of Computing & Biomedical Informatics
ISSN: 2710 - 1606
Volume 07 Issue 01
2024

Research Article
https://doi.org/10.56979/701/2024

Enhanced Skin Disease Diagnosis through Convolutional Neural Networks and Data Augmentation Techniques

Muddasar Abbas[1], Muhammad Arslan[2*], Rizwan Abid Bhatty[3], Fatima Yousaf[4], Ammar Ahmad Khan[5], and Abdul Rafay[5]

[1]Department of Department of Computer Science, Bahauddin Zakariya University, Multan, 60800, Pakistan.
[2]Department of Information Technology, Faculty of Computer Science, Lahore Garrison University, Lahore, 5400, Punjab, Pakistan.
[3]Department of Computer Science, University of Alabama at Birmingham, Birmingham, AL 35294, USA.
[4]Department of Computer Science & IT, Institute of Southern Punjab, Multan 60800, Pakistan.
[5]Department of Computer Science, NAMAL University, Mianwali,42250, Punjab, Pakistan.
[*]Corresponding Author: Muhammad Arslan. Email: marslan@lgu.edu.pk

Received: January 12, 2024 **Accepted:** May 26, 2024 **Published:** June 01, 2024

Abstract: Skin diseases are among the most common and widespread diseases affecting people around the world. Global warming and climate change are the two main factors leading to skin cancer. Skin diseases can be life-threatening if they are not detected and treated early. Clinical diagnosis of dermatological diseases is a relatively rare and expensive procedure, inaccessible to the general population. Advanced machine learning and image processing technologies enable feature extraction and disease identification. Deep learning is one of the emerging fields of machine learning that uses advanced intelligent techniques to classify images based on various features. In this research work multiple several deep learning models based on convolutional neural network (CNN) architecture such as sequential CNN model, DenseNet-121 and ResNet-50 are used for feature extraction. The HAM10000 dataset is used to evaluate the accuracy of the proposed model. There are 10015 images in the HAM10000 collection, which have been divided into seven different classes of skin diseases. The data set is divided into a training set and a test set, with ratios of 20% and 80%, respectively. Diagnosing skin diseases is a three-step process: first pre-processing the images of the dataset, then extracting features using CNN model in the second step and ends with classification of the skin disease category using various classifiers based on the features extracted in the third stage. Techniques for image augmentation were applied to lower the imbalance between different categories of skin diseases. The sequential CNN-based model with seven convolution layers achieves an accuracy of 98% and 99% for each of the seven categories of skin diseases in the Area Under the Curve (AUC). DenseNet-121 and ResNet-50 provide accuracy values of 89% and 84%, respectively. Various performance matrices are used to compare and evaluate the effectiveness of various CNN models on the provided dataset.

Keywords: CNN; Skin Cancer; Machine Learning; Deep Learning, ResNet-50; DesNet-121.

1. Introduction

Skin diseases are widespread worldwide, but they are particularly common in developing nations [1], [2]. Many factors such as excessive sun exposure, various blood contaminants, fungus, bacteria, viruses, and parasites can lead to various skin diseases [3]. Most skin diseases begin as abnormal skin growth that sometime develops into cancer in certain types of skin tissue. Benign and malignant skin disorders are the two main types of skin diseases [4]. MRI devices, X-ray machines, and laboratory examination of the affected skin area are the laboratory techniques used to diagnose skin disorders[5]. Trained specialists are needed to do the laboratory testing for the diagnosis of skin diseases. Most skin disorders have the same look, which makes it extremely challenging for a dermatologist to accurately diagnose the specific type of

skin disease relying just on laboratory test results and the visualization of affected regions. Dermatologists typically base their diagnosis opinions on skin visualization, which prompts more skin analysis and allows for laboratory skin analysis to validate the diagnosis [5]. When a medical emergency arises in developing nations without access to dermatologists in small cities or rural areas, relying solely on exports might provide significant challenges. The laboratory procedures require a large amount of electricity use, which can be problematic during the summer when electricity use rises.

Recent advances in medical technology based on images and laser technologies have increased the speed and accuracy of diagnosing skin diseases [6]. However, due to the high cost of these technologies, few hospitals can implement this approach. Recent advancement in science and technology allows us to diagnose skin diseases using computer-based models that classify skin diseases based on symptoms [7]. Machine learning and image processing are used to create computer-based systems for detecting skin diseases. These technologies are more accessible and easier to use for anyone with a computer or smartphone. Computer algorithms use image processing techniques to extract important features from skin disease images using machine learning [8]. Machine learning classifiers use features extracted from disease images to help categorize various types of skin conditions. The accuracy of machine learning classifiers is very high in providing high-quality and noise-free images.

Models based on deep learning can assist in resolving complex problems by detecting features in the input data [9]. The suggested model identifies skin diseases using CNNs. CNNs are powerful neural network models that have significant strengths for processing visual data [10]. Recently, CNN have shown exceptional performance in a range of medical applications, including object detection, face recognition, and image recognition [11–13]. The International Skin Imaging Collaboration (ISIC), an online archive of dermatological images, provides the dataset used in the proposed model [14]. More than 10,000 images represent seven different skin conditions, including dermatofibroma, benign keratosis-like lesions, vascular lesions, and melanocytic nevi. Actinic keratosis, basal cell carcinoma, melanoma and intraepithelial carcinoma are included in a dataset called HAM10000 [14], divided into training sets and testing using a set of random functions.

The main objective of the suggested research is to classify skin diseases using CNN by utilizing machine learning algorithms and image processing techniques. Additionally, the research aims to improve the accuracy of skin disease diagnosis by utilizing multiple techniques and reducing the number of false positives in the HAM10000 dataset. Finally, the accuracy of several CNN models, including DenseNet-121[15], and ResNet-50 [16], will be evaluated. Several matrices, including the f1 score, accuracy, precision, recall, loss, and classification report, are used to assess the suggested model.

The remaining sections of the research paper is divided as follows: section 2 reviews the literature, covering the most recent and relevant research on the topic. The proposed methodology and dataset visualization are covered in section 3. The results and the models' performance are presented in section 4. The conclusion of the research is covered in section 5.

2. Related Work

Skin disease identification is a major area of research due to the rapid advancements in deep learning and machine learning. This section presents recent work on skin disease detection from large-scale image data. Large volumes of image data can be processed using various deep learning algorithms and analyzed to identify specific patterns and indicators of skin disorders. In [17], the authors presented an efficient skin disease identification method using CNN, MobileNet and Xception architectures. The CNN architecture uses transfer learning techniques that involve pre-training a model on the ImageNet dataset to find additional features. In addition, the authors evaluate the performance of these methods using some widely used deep learning models, including DenseNet, InceptionV3, ResNet50, and Inception-ResNet. The study collected information on five different types of skin problems from two independent data sources. To evaluate the model's performance, various matrices measures such as precision, precision, recall, and F1 score were performed. The outcomes of experiments demonstrate this method's utilization. The classification accuracy of MobileNet reaches 96.00%, and the classification accuracy of Xception model using transfer learning reaches 97.00%.

S. Shivadekar et al. [18], presented the a hybrid multimodal engine based on bioinspired deep learning for prevention and post-treatment recommendations for dermatological diseases. The model provides

customized and precise recommendations to prevent and treat the effects of skin disorders by combining a number of techniques, such as analysis of the images, patterns of sleep, eating habits, and other clinical factors. This hybrid bionic technology combines elephant herd optimization (EHO) and antlion optimization (ALO) to enhance the reliability and accuracy of recommendations. The system uses natural language processing (NLP) and pattern mining to analyze a patient's medical history, and a binary cascaded convolutional neural network (BCCNN) to analyze skin disorder images. The model design consists of several modules adapted to the bionic optimization process, such as feature extraction, multimodal fusion, recommendation generation, and data preparation modules. An extensive image dataset is used to train and evaluate the model. of patient records and skin conditions. Experiments on medical samples demonstrate that the approach performs better than previous techniques.

In [1], A. Magdy et al. presented two methods to identify and classify benign and malignant tumors from images. The first method uses a pre-trained deep neural network based model to extract features and k-nearest neighbors (KNN) as a classifier. In the second, network hyperparameters are optimized using the Graywolf optimizer with AlexNet to improve efficiency of the model. In addition, the authors explore two skin cancer image classification methods: using deep learning (DL) and the broader filed machine learning (ML). Machine learning techniques include, KNN, support vector machines (SVM), naive Bayes, and decision trees. CNN and previously trained deep learning networks, like VGG-16, VGG19, and AlexNet.

In [19], a new technique for skin disease detection was proposed in which non-standard images from a traditional camera are captured and combined using multiple angles, such as close-ups that highlight specific lesions and long shots that include the background of the surface of the body. Computer-aided diagnosis (CAD) models trained utilizing non-standard traditional images typically presents poorer results compared to CAD models that identify localized disorder of a small area, like dermoscopic images. The model creates a CAD dataset of skin disease images that can be used to classify multiple skin diseases by creating a skin image segmentation model based on CNN. To identify skin and wound regions, the authors trained a CNN segmentation model based on DeepLabv3, then identified areas that met the following criteria: The percentage of skin area and wound area in an image should be greater than 80% and 10%, respectively. The dataset of segmented images produced by CNN was analyzed using computer aided diagnosis (CAD) to classify dermatological diseases.

In [8], the authors presented a new framework for automated diagnosis of different skin disorders by using segmentation and classification algorithms for skin lesions. Classification and segmentation of lesions and pre-processing are important steps in the provided approach. Firstly, the image is prepared for efficient classification by performing contrast enhancement, hair removal, and grey-level conversion. Following image pre-processing, the upgraded U-Net segmentation method is used to segment skin lesions. This enhancement is achieved by recommending a hybrid algorithm. In addition, the proposed hybridized optimization algorithm may solve a finite collection of problems in addition to solving local optimal problems. The combination of optimization techniques balances search and exploitation capabilities through its simplicity, global optimal search capabilities, and faster convergence. An optimized ensemble convolutional neural network (E-CNN) then completes the classification. CNN uses five independent expert systems instead of its own fully connected layers to classify skin diseases. During the classification phase, the system also optimized several parameters to improve processing efficiency and reduce network complexity. The segmentation and classification problems are optimized using a hybrid metaheuristic method called wheeled electric fish optimization (W-EFO), which is based on EFO and wheeled optimization techniques.

Moreover, K. V. Swamy et al. [20], proposed another technique for skin disease identification. In the medical field, ML methods are widely used for diagnostics. These ML algorithms take image feature as input and use them to determine the output. The process is divided into three stages: feature extraction, training and testing. The method uses different sets of skin images to train itself using machine learning techniques. Texture, color and shape, and their combination, are the three main factors in image classification. This article categorizes skin conditions based on criteria related to color and texture. Healthy skin has a different color than diseased skin. Texture elements in images are an effective way to determine regularity, smoothness, and roughness. For accurate diagnosis of skin diseases, these two aspects are discussed. In this work, the maximum histogram value, variance and entropy of the Hue Saturation Value (HSV)

function are used. These functions are used to build deep learning-based algorithms using support vector machines (SVMs) and decision trees (DTs). Partition the tree at the first level using the entropy measure. Use mutations at the second level to obtain the leaf structure. The maximum histogram value of the HSV metric is used for color features for tree segmentation.

In [21], a neural network based model for skin disease identification was presented. The authors proposed a unique multimodal transformer consisting of two image and metadata encoders and a decoder to combine multimodal information as the research dataset is skin disease images and medical metadata. The core of the network model is a suitable Visual Transducer (ViT) model for extracting depth information from images. Metadata is processed as tags and embedded using the new Soft Tag Encoder (SLE). In addition, a mutual attention (MA) block is introduced in the decoder part to improve the integration of image features and metadata information.

Table 1. Comparison Table of previous Skin detection Techniques

Authors/Reference	Techniques/Model	Limitations
R. Sadik et al[17] 2023	Convolutional Neural Networks (CNN) - MobileNet, Xception, ResNet50, InceptionV3, Inception-ResNet, DenseNet	Low contrast and visual similarity between different conditions; reliance on transfer learning and data augmentation; specific to the data used; potential generalization issues.
A. Magdy et al [1] 2023	k-nearest neighbor (KNN), various ML and DL approaches including CNN, AlexNet, VGG-16, VGG-19, ResNet-18	Complexity of integrating multiple models; high computational requirements; dependency on quality and variability of training dataset; challenges with hyperparameter optimization
D. A. Reddy [8] 2023	Enhanced U-Net for segmentation, Ensemble-CNN for classification (Random Forest, ANN, SVM, Adaboost, XGBoost), Whale-Electric Fish Optimization (W-EFO)	Complex computation and tuning of parameters; challenges with poor extraction of skin lesions; potential issues with generalization and overfitting; dependency on preprocessing steps
S. Shivadekar [18] 2023	Binary Cascaded Convolutional Neural Network (BCCNN), NLP with pattern analysis, Elephant Herding Optimization (EHO),	Complexity of integrating multiple modalities; reliance on accurate patient data; bioinspired optimization methods may be

		computationally intensive
Y. Yanagisawa [19] 2023	DeepLabv3+-based CNN for segmentation, CAD for skin disease classification	Performance dependency on image quality; potential issues with variability in image fields; needs consistent image dataset quality for optimal performance.
K. V. Swamy [20] 2023	Support Vector Machine (SVM),Decision Tree (DT),	Difficulty in handling hair on skin, varied skin textures, and colors; dependency on feature extraction accuracy; limited by the specific features used (HSV, entropy, variance)
G. Cai [21] 2023	Vision Transformer (ViT), Soft Label Encoder (SLE), Mutual Attention (MA) block	Dependency on high-quality and diverse datasets; complexity in integrating and tuning multimodal data; potential challenges with real-time application and computational resources

3. Materials and Methods

Dermatologists face difficulties in the early detection of skin cancer. The steps of the proposed methodology are dataset, preprocessing, feature extraction, data augmentation, model training, image segmentation into training and test data sets, and skin disease classification. The complete methodology is shown in figure 1 and data flow of proposed model is shown in figure 2.

3.1. Dataset Description

The small size and insufficient diversity of skin disease datasets provided have a significant impact on the training process of many neural networks used for automatic diagnosis of skin disease. A subset of the ISIC archive used was the HAM10000 dataset, which contains 10015 images of seven different skin conditions. HAM10000 is derived from the ISIC repository, which is considered a compilation of several dermatoscopy datasets containing 23665 images of various skin conditions[22]. HAM10000 optimizes automated methods for testing and training models based on neural networks.

3.2 Data visualization

Preprocessing is the process of modifying data before sending it to the algorithm [23]. Preprocessing transforms raw data into a clean collection of data. In other words, information collected from many sources is often obtained in raw form and is not suitable for verification. Data visualization is the process of presenting information and data graphically [24]. The focus of the proposed model is to analyze the current data on various skin diseases and develop a reliable system for early identification of types of skin diseases that will help patients in the early stages of their development. This section uses various data visualization techniques to graphically present information about skin diseases to create awareness about different types of skin diseases.

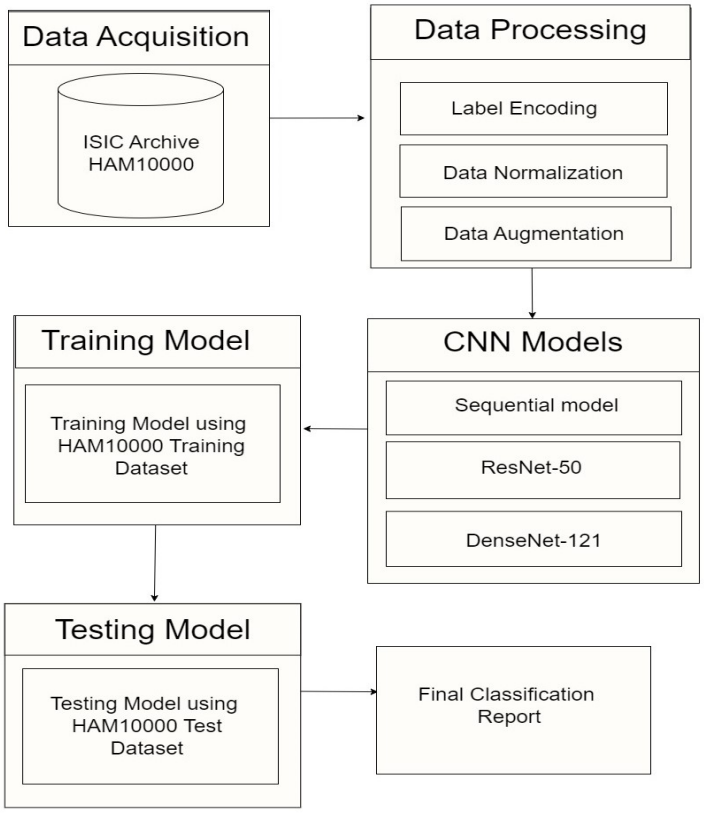

Figure 1. Proposed model architecture

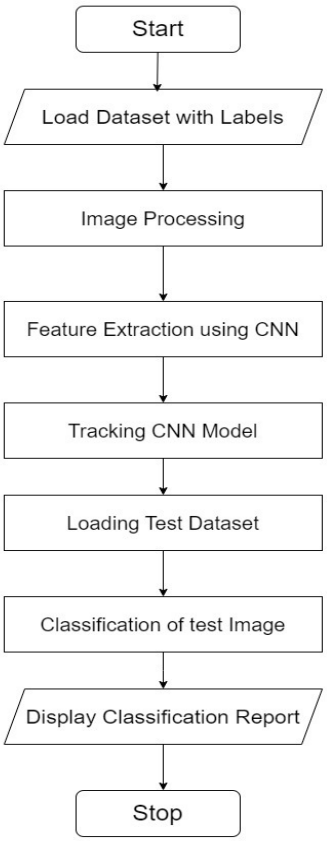

Figure 2. Data flow of the proposed model

Visualization tools present data graphically to make it easier to understand. It includes various graphical and statistical descriptions of the data in the dataset used for this method [24]. The distribution of the 7 classes of the skin disease included in the HAM100000 dataset is shown in the histogram in Figure 3. The most common skin condition is called melanocytic nevus or nevus. The symbols for melanoma, basal cell carcinoma, vasculoderma, dermatofibroma, actinic keratosi are represented by the letters mel, bcc, vasc, df, akiec respectively.

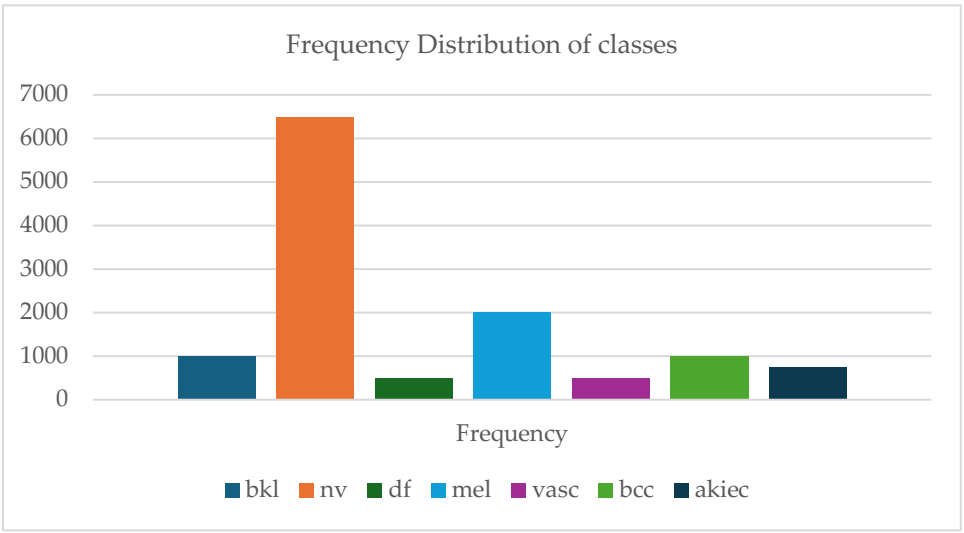

Figure 3. Distribution Frequency for different classes of skin diseases

The frequency distribution of the HAM10000 dataset shows an imbalance. Most dermatological categories have fewer than 10,000 samples. Only three groups had more than 1000 samples: melanocytic nevi, benign keratoses, and melanoma. As this frequency distribution shows, melanocytic dermatoses are the most common skin diseases worldwide. If there are not enough samples to train, the model may have lower predictive performance for skin disease categories. Resampling techniques aim to standardize the data set and increase the number of samples [25]. Figure 4 displays a pie chart that illustrates the prevalence of skin conditions according to the patient's gender. The patient may identify as male, female, or another gender.

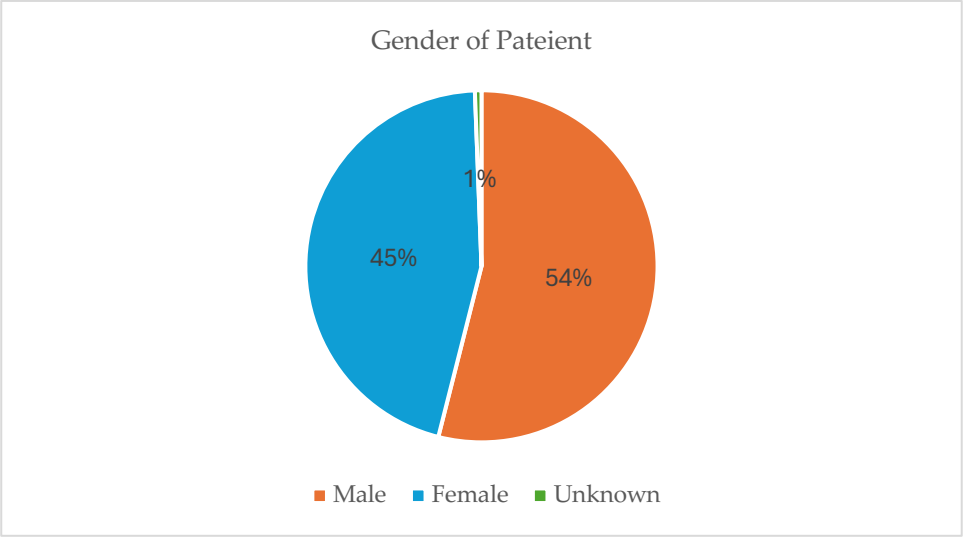

Figure 4. Pie chart showing patient gender

Figure 4's pie chart illustrates that skin illnesses are more common in men than in women and other gender groups. The percentage of male patients with skin illnesses is 54% of all skin disease patients. About 45.5% of patients with any kind of skin illness are female. In the HAM10000 dataset, the proportion of other patients is 0.6 percent. A histogram depicting the frequency distribution of skin conditions throughout patient age is displayed in figure 5.

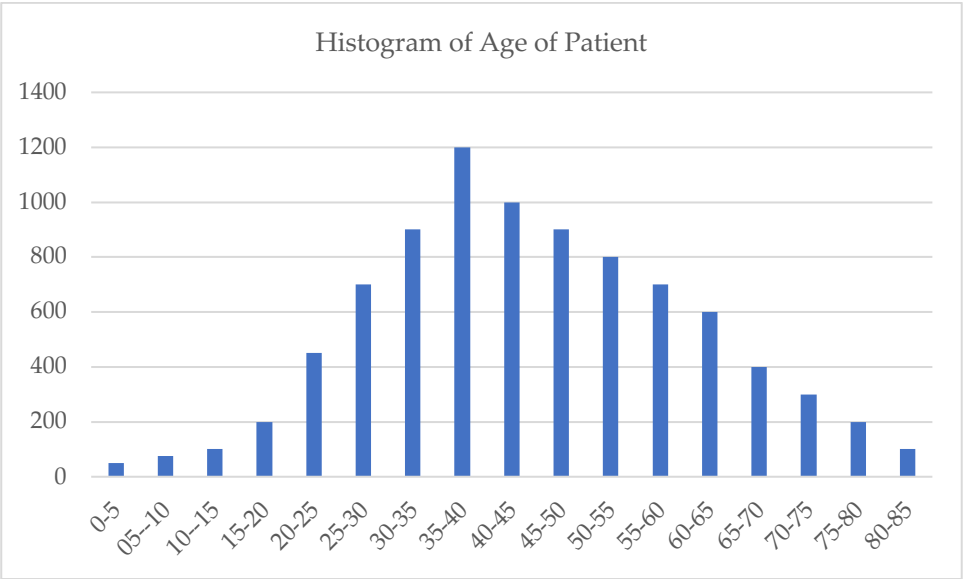

Figure 5. Skin Disease distribution with the age of the patient

Figure 5 shows the distribution of skin diseases across various body sections as a bar graph. Gender is another factor that the bar graph employs to paint a fuller picture of the distribution of various skin

disorders across the body parts of humans. The patient's gender is shown by various colored bars in the bar graph.

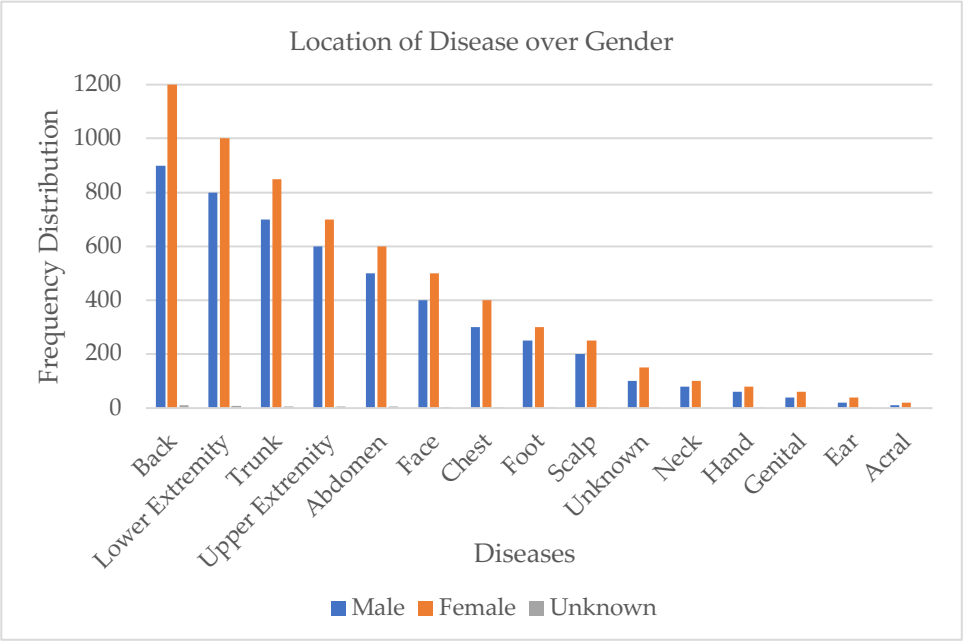

Figure 6. Skin Disease distribution with the age of the patient

3.3. Data preprocessing

For a sequential CNN model, all images must be of a certain size. All images must be converted to 256*256 size. The size of the input data changes according to the classification model. The default image size of DenseNet-121 is 224*224 [26]. Seven classes are produced using the data extracted from the HAM10000 dataset; a number between 0 and 6 indicates each class. Each of the nine kinds of skin diseases in the ISIC dataset is represented by a number between 0 and 8. Data normalization is a strategy that reduces the overall number of training times while normalizing input data [27]. To normalize the input data, the mean and standard deviation are calculated. Because melanoma and melanocytic nevi, two skin disease categories with varying numbers of samples, are predominantly represented in the dataset, oversampling is utilized to minimize this variation. The dataset is more balanced because the remaining skin disease categories have more samples due to oversampling. The following equation is utilized to compute the mean and standard deviation [28]:

$$\mu = \frac{1}{N}\sum_{i=1}^{N} x_i \quad (1)$$

$$\sigma = \sqrt{\frac{1}{N}\sum_{i=1}^{N}(x_i - \mu)^2} \quad (2)$$

In this case μ represents mean, $\sum_{i=1}^{N}$ represents the sum ranging from 1 to nth value. σ represents standard deviation.

3.4. Data Augmentation

The training dataset is artificially expanded using data augmentation. It entails creating altered versions of the dataset's images. [29]. Deep learning-based models' prediction performance is strongly influenced by the size of the dataset; a model with more data may predict things more accurately than a model with less data. By producing multiple versions of the same image, the data augmentation technique enhances a model's capacity to apply what it has learned to new images [30]. When there are insufficient training samples and the model becomes overfit, the data augmentation technique is frequently employed. Most of the images in the HAM10000 dataset come from the melanocytic classes of skin illnesses, which increases the possibility of overfitting the model while projecting a rise in other classes of skin diseases for which there is a dearth of training data. The deep learning Keras package makes it possible to automatically apply data augmentation during model training. This is accomplished by utilizing an already-existing ImageDataGenerator class. The class is initialized, and the class constructor is debated with respect to the types of data augmentation techniques in the first stage.

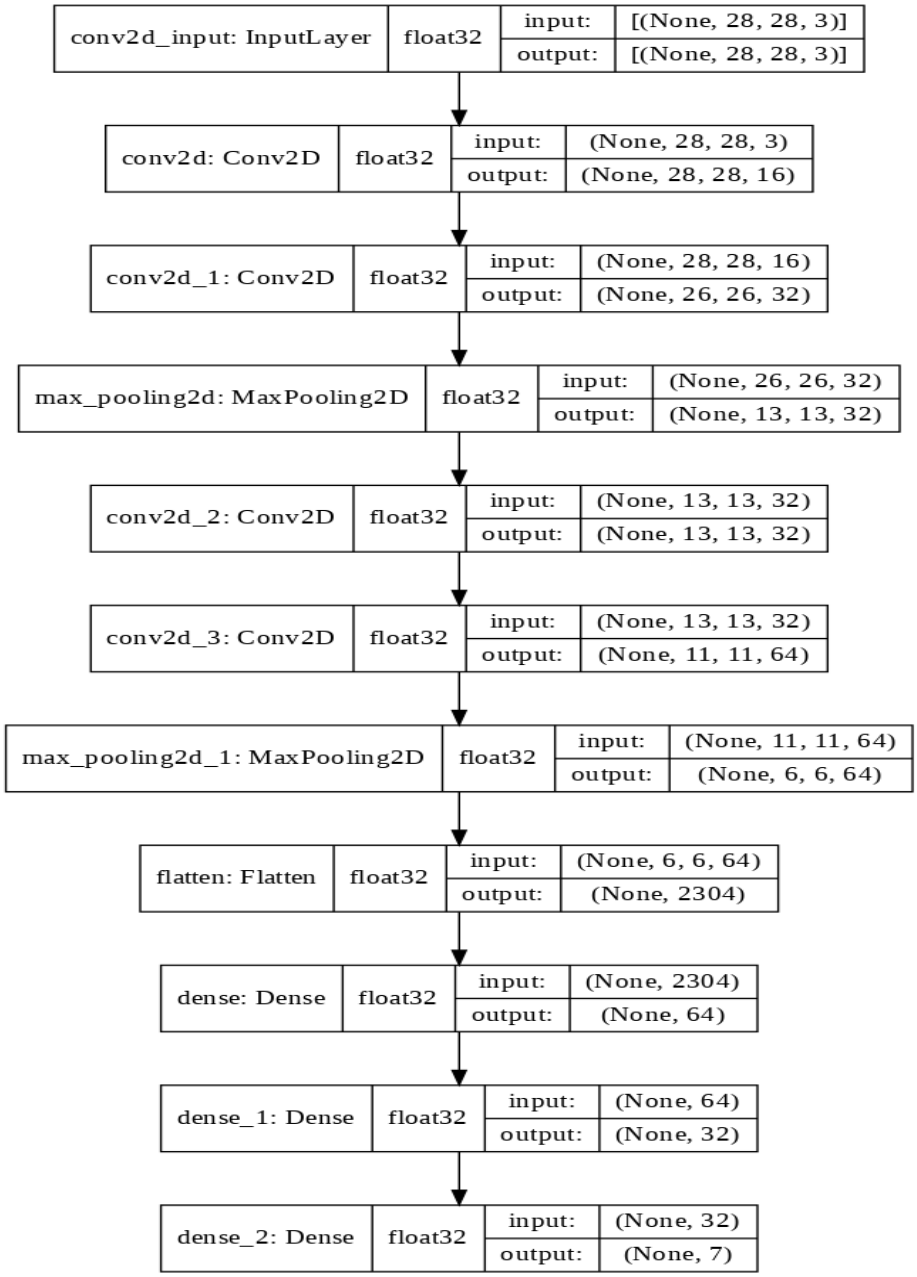

Figure 7. Proposed model with sequential approach

Many different strategies are supported by the data augmentation method. The following five types of data augmentation techniques are employed in this proposed model:

3.4.1. Scaling

The purpose of scaling is to modify the size of images stored in a database to improve performance and flexibility of the training data [31]. Scaling allows images to be doubled in length or width to make them larger. Images can be made smaller than their original size by shrinking or scaling them [32]. For this, the Resize () function is utilized, which takes as input the size of the resulting image.

3.4.2. Cropping

Cropping is a data augmentation technique that involves removing some part of the image to enhance the clarity and accuracy of an image [33]. Center cropping is a technique used to augment data to eliminate pixels from an image that do not provide important information about skin conditions. The main goal is to keep the important portion of an image only and remove unnecessary portion of the image. Cropping an image helps create more variations of the original image.

3.4.3. Flipping

As part of a data augmentation approach called flipping, an image is flipped vertically or horizontally to create more image variants for the model's training and to lessen the overfitting issue [34]. This technique

allows to create additional variants of an image by flipping to secure the informative portion of an image. Flipping helps CNN models to train extraction of features from an image despite change of orientation.

3.4.4. Padding

The purpose of padding is to make numerous copies of a single image and enlarge it. Padding involves filling in the image's designated borders on all sides with varying values [35]. Using the transforms.pad() function is how padding is done. This technique involves creating multiple variants of images by adding additional pixels along the border of images. It helps to enhance diversity of datasets and improves accuracy by training CNN models on multiple variants of images.

3.4.5. Rotation

Another technique employed in image augmentation is rotation. The image is rotated to a specified angle, either clockwise or counterclockwise [36]. Rotating an image can provide a large number of different visual variations, all of which are beneficial for effectively training the model and avoiding overfitting.

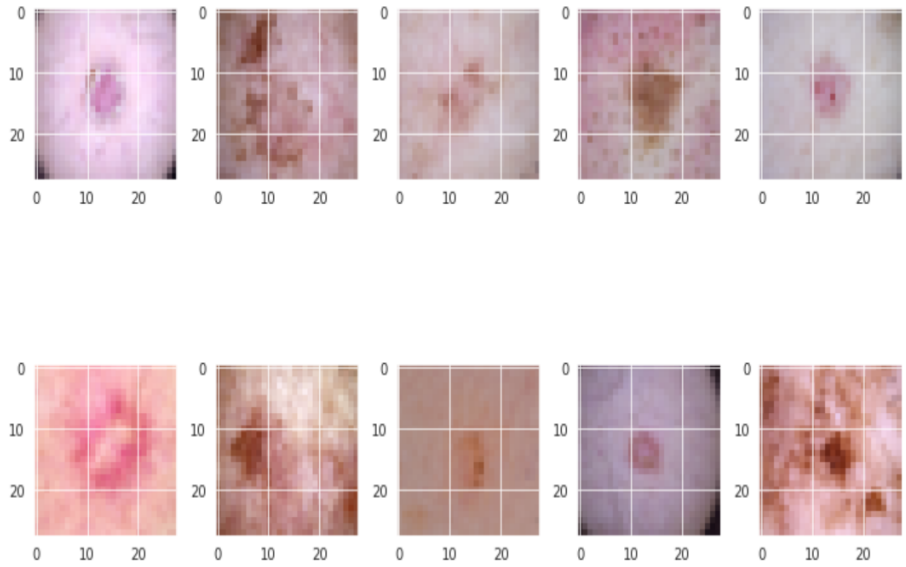

Figure 8. Random Dataset images after training

3.5. Model Implementation

Deep learning is a subfield of ML that uses several layers for extraction of higher-level features from input images. Higher-level layers of CNN are used in image processing to identify various concepts for classification, whereas lower-level layers are utilized to identify edges [37]. A series of convolutional, pooling, nonlinear, and fully linked layers are used by the CNN model [38]. The sequential model is applied in this proposed research. One of the simplest methods for creating a model with Keras is sequential. With this method, we can create our own model by gradually adding layers one after the other. The model can have additional layers added by using the add() function. The sequential approach model employed in this work is depicted in Figure 7. The model in figure 3.11 takes a 28 × 28 x 3 image size. The maxpooling2D layer comes after the first two conv2D levels in the model. The model employs layers of maxpooling2D and conv2D in various combinations. ReLu is used as a function of activation in the first two layers [39].

$$y = \max(0, x) \qquad (3)$$

SoftMax serves as an activated function in this model, and the dense layer served as the output layer. Since the SoftMax produces a series range from 0 and 1 that combines to 1, the SoftMax activation function is utilized [40].

$$\sigma(z)_i = \frac{e^{z_i}}{\sum_{j=1}^{K} e^{z_j}} \qquad (4)$$

Utilizing an optimizer, the model's learning rate is managed. The Adam optimizer is used in this work [41]. While training the model, optimizer Adam is used to modify the learning rate. In this case, the rate at which model weights are calculated is determined by the learning rate. More accurate weights are obtained with a reduced learning rate, but the weights' computation time rises. Training accuracy results are displayed using the accuracy metric. Categorical_Crossentropy is the loss function employed in this paper. For multiclass classification, this is the most often utilized loss function. A lower score denotes a higher model performance.

4. Results and Evaluations

The results of the suggested model are analyzed and evaluated in this section utilizing various matrices. The HAM10000 dataset is used to train the CNN model, which is based on the multiclass classification model. Several measures, including validation and training loss as well as training accuracy and validation accuracy, are utilized to assess the models' output. The CNN model's capabilities can be determined with the help of these parameters. The model's performance is evaluated using three primary techniques: precision, accuracy, and sensitivity. A variety of assessment matrices are used to assess the model's performance.

4.1. Confusion Matrix

One of the most popular matrices to display a model's recall and precision is the confusion matrix [42]. A classification problem's estimated outcomes are summarized in the confusion matrix. A method to identify areas where the model makes mistakes and what it is doing correctly is to use the confusion matrix. The predictive class shows the values that were predicted using the model, whereas the real values are displayed in the actual class. A model's accuracy is determined by maximizing the true positives (TF) and minimizing the false negatives (FN), as well as by maximizing the positives (FP) and FN [43]. These four elements support the model analysis.

4.2. Accuracy

The machine learning classification model's performance is measured by its accuracy [44]. The total number of accurate predictions by the proposed model divided by the total number of model predictions yields the classification model's accuracy. The best indication of a model's performance on a given dataset is provided by accuracy. When the database is balanced, the best accuracy ratings should be anticipated. Because the dataset is balanced, almost equal numbers of objects are available for each class to use in model training.

$$\text{accuracy} = \frac{\text{TN+TP}}{\text{TN+FN+FP+TN}} \qquad (5)$$

In this case, TN indicates true negative, TP indicates true positive, FP presents false positive, and FN indicates false negative.

Table 2. Model training for 25 Epoch

Epoch	Training Loss	Training Accuracy	Val_Loss	Val_Accuracy	Time (s)
1	3.6042e-04	1.0000	0.0721	0.9861	9s 32ms
2	3.2981e-04	1.0000	0.0702	0.9870	9s 31ms
3	3.1452e-04	1.0000	0.0740	0.9867	9s 31ms
4	2.7877e-04	1.0000	0.0704	0.9871	9s 32ms
5	3.0605e-04	1.0000	0.0723	0.9869	9s 31ms
6	2.7565e-04	1.0000	0.0702	0.9870	9s 31ms
7	2.8275e-04	1.0000	0.0728	0.9869	8s 31ms
8	2.4404e-04	1.0000	0.0723	0.9869	9s 31ms
9	2.5718e-04	1.0000	0.0704	0.9876	9s 31ms
10	2.5652e-04	1.0000	0.0710	0.9871	9s 32ms
11	2.5818e-04	1.0000	0.0711	0.9872	9s 33ms
12	2.4980e-04	1.0000	0.0720	0.9867	9s 32ms
13	2.4274e-04	1.0000	0.0688	0.9878	9s 32ms
14	2.8260e-04	0.9999	0.0688	0.9877	9s 33ms
15	2.4937e-04	0.9999	0.0682	0.9879	9s 33ms
16	2.2046e-04	1.0000	0.0709	0.9871	9s 32ms
17	2.1862e-04	1.0000	0.0695	0.9877	9s 32ms
18	2.0453e-04	1.0000	0.0717	0.9875	9s 32ms
19	1.8431e-04	1.0000	0.0738	0.9865	9s 33ms
20	2.1444e-04	1.0000	0.0690	0.9879	9s 32ms
21	1.8681e-04	1.0000	0.0704	0.9876	9s 32ms
22	1.9542e-04	1.0000	0.0713	0.9876	9s 31ms
23	1.9970e-04	1.0000	0.0724	0.9876	9s 31ms
24	1.9763e-04	1.0000	0.0704	0.9882	9s 32ms
25	1.7334e-04	1.0000	0.0719	0.9875	9s 32ms

There are two other categories of model accuracy: testing accuracy and training accuracy. The training accuracy of a model is its accuracy across the training dataset. The validation accuracy is the accuracy of the model over the testing or validation dataset. The accuracy curves for training, testing, and validation of the suggested model using the CNN sequential technique are displayed in Figure 9.

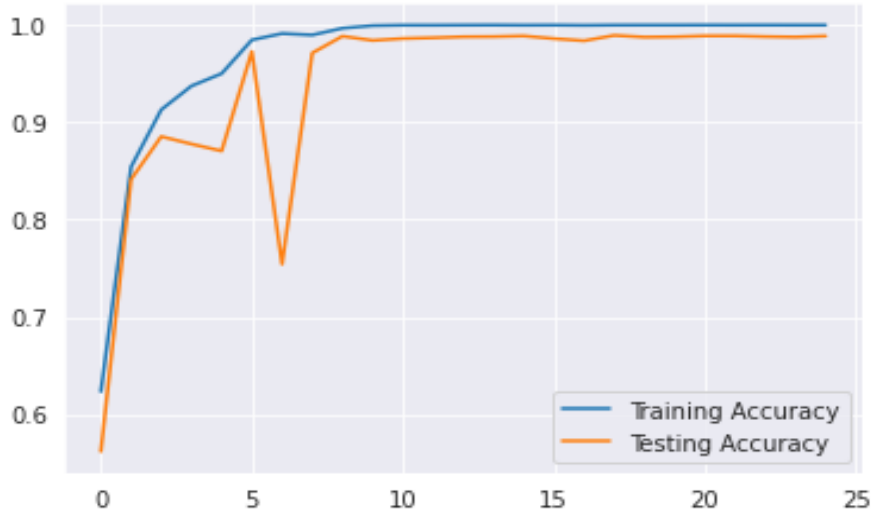

Figure 9. Training and testing accuracy of proposed model

The execution of the proposed model using an available training dataset is shown by the training accuracy. The accuracy of the validation or testing process indicates how effectively the model will function when applied to a fresh dataset. When applied to the training dataset, the first suggested model yields 100% accuracy; when applied to the validation or testing dataset, it yields 98% accuracy.

4.3. Training Loss

Another indicator of the model's performance is the loss function. The classification model is optimized using the loss function. The loss is calculated using the validation/testing and training datasets. The loss indicates the model's effectiveness on a particular dataset. The loss is the error that suggested method produces while using training or validation datasets. The loss indicates the model's performance after each iteration, either poorly or well. The proposed model uses the loss function to find the difference between predicted values by the model and the actual target values. The loss function is used to differentiate between actual output and predicted output by the model [45].

$$H_p(q) = \sum_{i=1}^{N} \sum_{j=1}^{C} y_{ij} \log (p_{ij}) \qquad (6)$$

In this case $H_p(q)$ indicates loss function, C represents the total no of classes. Figure 9 shows the training, testing, and validation loss curves for the proposed model. The validation loss in the suggested model, which employs a sequential approach based on CNN, is less than 0.05, and the training loss is nearly negligible.

4.4. Classification Report

The accuracy of a classification model's predictions is displayed in the classification report. The classification report serves as a matrix for assessing a classification model's performance. The proposed classification model's recall, precision, f1-score, and support are displayed in the classification report. An improved overview of the classification model's performance is provided by the classification. The f1-score, recall, and accuracy values for each class in the classifier model are displayed in the classification report. To use categorization reports, import the SK-learn package into Python.

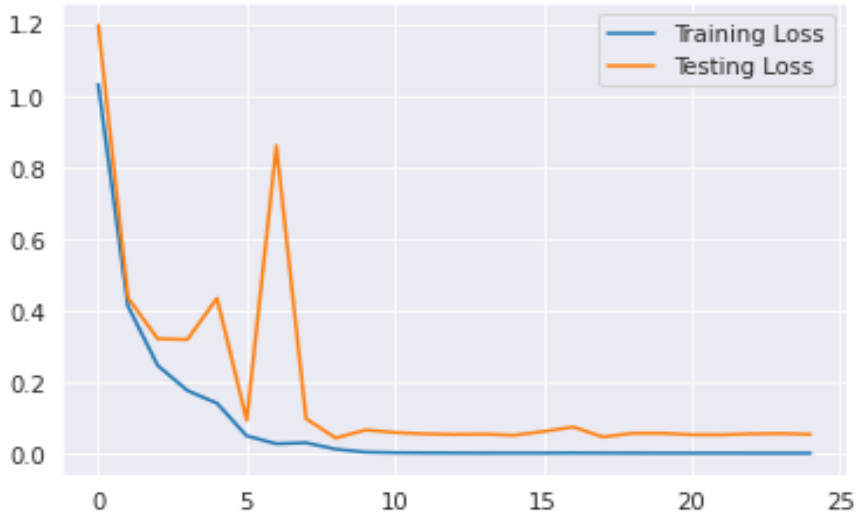

Figure 10. Training and testing loss of proposed model

.

The report provides a classification of the model's precision, f1-score, and recall values for seven classes of skin diseases: melanocytic nevi (NV), vascular lesions (VASC), actinic keratoses (AKIEC), dermatofibroma (DF), basal cell carcinoma (BCC), and melanoma (MEL). Additionally, weighted, sample, macro, and micro averages are included in the classification report. Figure 10 displays the categorization report for the suggested model.

	precision	recall	f1-score	support
('akiec', 'Actinic keratoses and intraepithelial carcinomae')	1.00	1.00	1.00	1667
('bcc', ' basal cell carcinoma')	0.99	1.00	1.00	1689
('bkl', 'benign keratosis-like lesions')	0.97	1.00	0.98	1651
('df', 'dermatofibroma')	1.00	1.00	1.00	1629
('nv', ' melanocytic nevi')	1.00	0.94	0.97	1663
('vasc', ' pyogenic granulomas and hemorrhage')	1.00	1.00	1.00	1680
('mel', 'melanoma')	0.97	0.99	0.98	1755
micro avg	0.99	0.99	0.99	11734
macro avg	0.99	0.99	0.99	11734
weighted avg	0.99	0.99	0.99	11734
samples avg	0.99	0.99	0.99	11734

Figure 11. Proposed CNN classification model classification report

4.5. Precision

The precision of the classification model lies in its capacity to accurately identify only pertinent data items. The percentage of the pertinent results is displayed by precision. The ratio between the total number of true positives and false positives and the total number of true positives is the model person. Precision demonstrates the model's prediction accuracy. The suggested model accurately predicts the four types of skin diseases: vascular lesions (VASC), basal cell carcinoma (BCC), dermatofibroma (DF), and actinic keratosis (AKIEC). The suggested model has a precision score of 0.95 for benign keratosis (BKL), 0.97 for melanoma (ML), and 0.99 for melanocytic nevi (NV) [46].

$$\text{Percision} = \frac{\text{TP}}{\text{FP+TP}} \qquad (7)$$

4.6. Recall

The model's recall refers to its ability to accurately identify true positives. Recall is the total number of true positives divided by the total number of false negatives and true positives. More accuracy can be achieved with classification models that have a greater recall value. In our suggested model, the recall value is 1 for the first five categories of skin illnesses and 0.92 and 0.99 for the last two categories, respectively. The recall calculation equation is shown below [47].

$$\text{Recall} = \frac{\text{TP}}{\text{FN+TP}} \qquad (8)$$

4.7. F1-Score

F-score is a common term for the F1-score. In mathematics, the F1-score is a weighted mean of the classification algorithm's recall and precision. The value of the F1-score ranges from 1 to 0. The F1-score is influenced similarly by recall and precision. The values of the F1 score show how accurate a classification model is on a given dataset. The formula for computing the F1-score is displayed below. [48].

$$F1 - \text{Score} = 2\frac{(P*R)}{(R+P)} \quad (9)$$

In this case P indicates precision and R indicates recall ratios.

4.8. Support

The genuine number of instances of a particular class in the provided dataset is represented by the term support in classification. The training dataset's support imbalance can point to a serious flaw in the classifier's predicted scores and point to the need for stratified sampling or rebalancing. The model's classification has no effect on the degree of support. Every class in the database has support values that are almost equal and above 1600.

4.9. ROC Curve

The capacity of the proposed model for prediction is represented graphically by the Receiver Operating Characteristic (ROC). The classification model's performance at various intervals is displayed on the ROC curve. These days, the ROC curves are being utilized in machine learning, radiology, and other domains. Plotting false-positive rates against true-positive rates is done using the ROC curve. True positives are the percentage of total forecasts, out of all positive observations, that the model correctly forecasted as positive. Plotting TPR and FPR at various points throughout a model's classification phase is done using the Roc curve. The ROC curve analysis provides a way to choose potentially optimal classification models and eliminate below average models independently from the class distribution. When making analytical decisions, the ROC curve analysis provides a simple and reliable measure of benefit/cost analysis. The link between specificity and sensitivity is displayed by the ROC curve advancement. Any random classifier is used as a starting point to assign points that are adjacent to the x-axis (FPR = TPR). The curve indicates that the accuracy of the model is decreasing as it bends towards an angle of 45 degrees from the diagonal. The ROC curve for the suggested model using the HAM10000 dataset is displayed in figure 12.

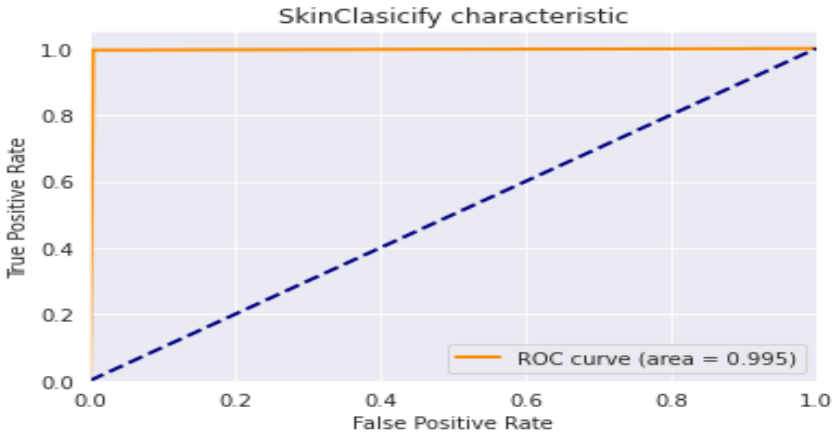

Figure 12. ROC of the sequential CNN model

4.10. Model Performance

4.10.1. Resnet-50

The training dataset generates an accuracy of 0.90187 for the Resnet-50-based model, whereas the validation dataset yields an accuracy of 0.8438. The distribution of the HAM10000 dataset is 20% for the training dataset and 80% for the validation dataset. When there are differences in the quantity of samples available for training and testing, the model's accuracy in diagnosing various skin conditions differs. The graph of the Resnet-50 model's testing and training loss, along with validation and training accuracy, is displayed in Figure 13.

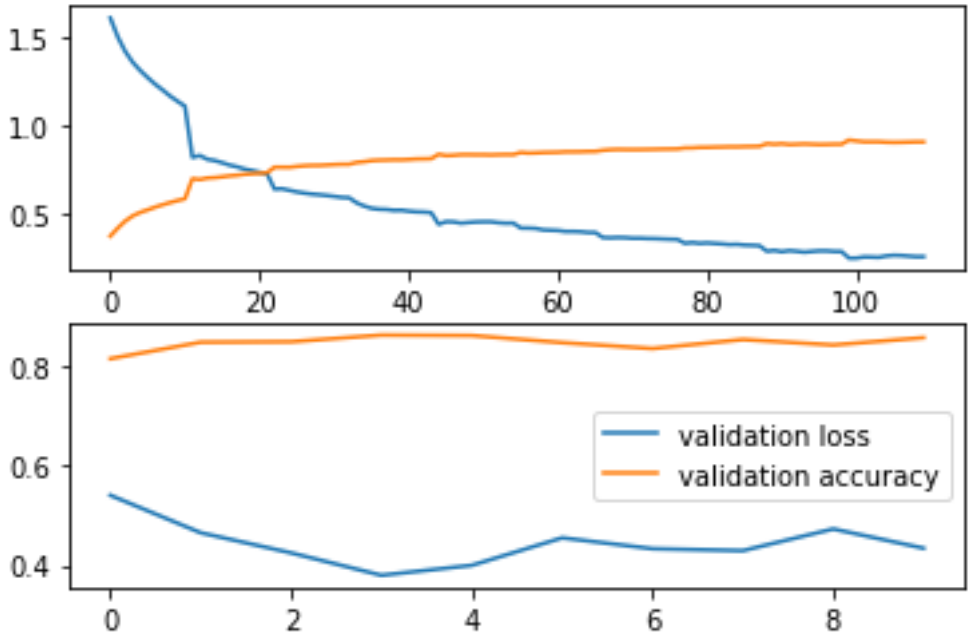

Figure 13. Accuracy, validation and training loss for Resnet50-based model

The Resnet-50 based model's confusion matrix and classification report, which provide specifics about the model's performance over ten epochs, are provided below. The confusion matrix for the model based on Resnet-50 is displayed in Figure 14 and classification report is shown in figure 15.

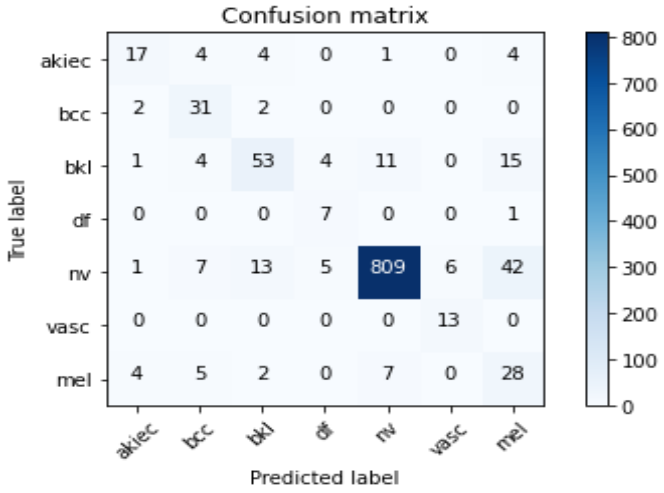

Figure 14. Confusion matrix of resnet50 model

	precision	recall	f1-score	support
akiec	0.68	0.57	0.62	30
bcc	0.61	0.89	0.72	35
bkl	0.72	0.60	0.65	88
df	0.44	0.88	0.58	8
nv	0.98	0.92	0.95	883
vasc	0.68	1.00	0.81	13
mel	0.31	0.61	0.41	46
accuracy			0.87	1103
macro avg	0.63	0.78	0.68	1103
weighted avg	0.90	0.87	0.88	1103

Figure 15. Resnet-50 classification report

The precision and recall levels of the model's classification report vary according to the various skin disease categories. In comparison to other skin disease categories such as melanocytic nevi (NV), the quantity of training and validation samples for melanoma (ML) and dermatofibroma (DF) is quite low, which results in very poor precision values. Increasing the number of training dataset samples helps in improving the accuracy of the model.

4.10.2. DenseNet121

On the training dataset, the DenseNet121-based model's accuracy is 0.93028, while on the testing dataset, it is 0.89274. The ratio of the testing to training datasets is 20% and 80%, respectively.

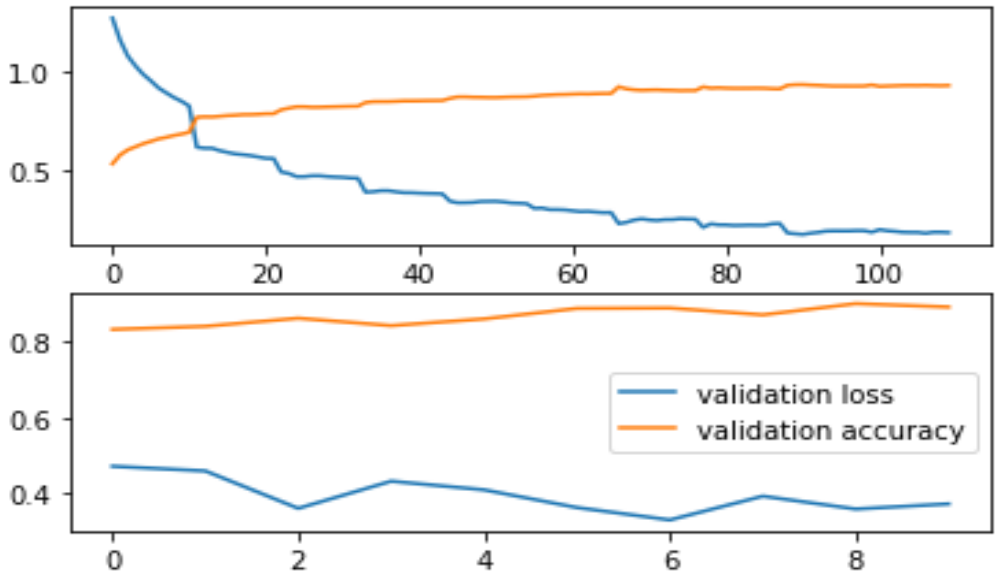

Figure 16. Densenet121 training and testing accuracy and loss

The accuracy levels within the validation dataset exhibit variability between several categories of skin diseases, wherein the quantity of training samples is not uniform. The loss and accuracy curves for the training and testing datasets are displayed in Figure 16.

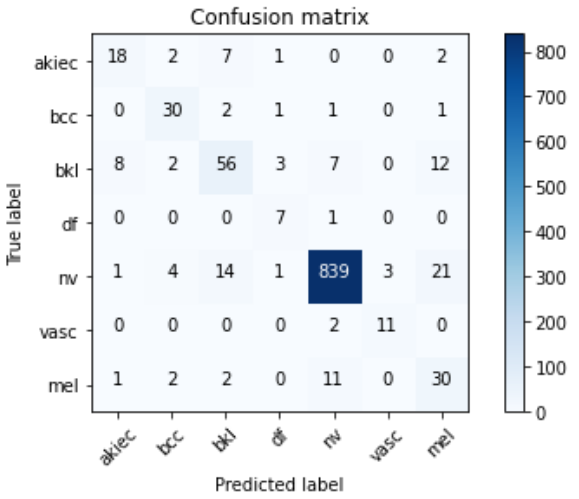

Figure 17. Densenet121 Confusion Matrix

	precision	recall	f1-score	support
akiec	0.64	0.60	0.62	30
bcc	0.75	0.86	0.80	35
bkl	0.69	0.64	0.66	88
df	0.54	0.88	0.67	8
nv	0.97	0.95	0.96	883
vasc	0.79	0.85	0.81	13
mel	0.45	0.65	0.54	46
accuracy			0.90	1103
macro avg	0.69	0.77	0.72	1103
weighted avg	0.91	0.90	0.90	1103

Figure 18. DesneNet121 classification report

The HAM10000 dataset's categorization report displays differences in precision and recall levels for every type of skin condition. Precision ratings of greater than 60% are found in most groups of skin diseases. Different numbers of samples are included in the dataset for each type of skin condition; therefore, precision and recall fluctuate between them.

4.10.2. Sequential CNN Model

On the training dataset, the CNN model's accuracy was 0.9686, whereas on the test or validation dataset, it was 0.9561. On the training dataset, the CNN model's accuracy is 1.0; however, on the testing the value is 0.9878, following the addition of seven convolutional layers in place of four and the application of batch normalization. Figure 19 displays the accuracy of the suggested model on training and testing sets both before and after layer improvements.

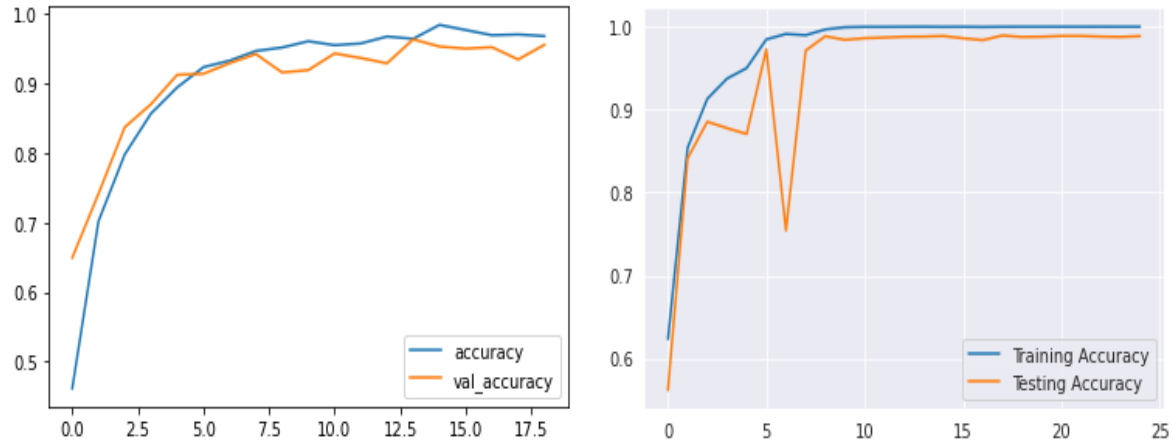

Figure 19. Accuracy of CNN Model before and after changing layers

Figure 19 shows the model's training accuracy and validation accuracy on the left side before enhancing its layered structure, and on the right side following the application of the enhanced layered structure with batch normalization. Figure 20 displays the classification reports for the CNN model both with and without the revised layer structure.

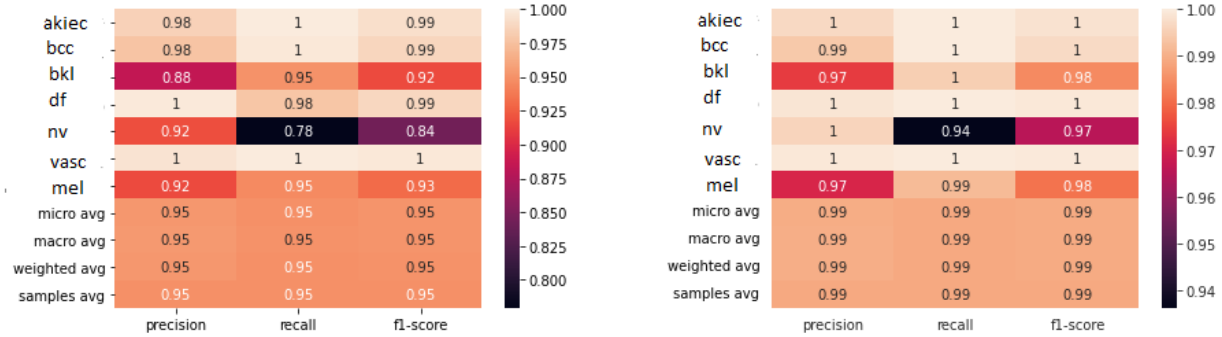

Figure 20. The proposed CNN model's classification report

The categorization report indicates that the skin disease categories with fewer training sample counts have improved in precision and recall. There has been a noticeable improvement in the precision and recall levels for each category of skin condition. The CNN model's confusion matrix is displayed in Figure 21 both before and after batch normalization and layer changes.

Figure 21 shows the confusion matrix on the left side before layer optimization and the confusion matrix on the right-side following layer optimization. A significant improvement in the model's prediction accuracy is evident. In practically every class of skin disease, the total number of true positives rises while the total number of false positives falls. Prior to optimization, the CNN model could accurately predict roughly 1300 samples for each type of skin illness found in the HAM10000 dataset.

4.11. Comparison of various CNN models using the HAM10000 dataset

This paper uses three different CNN models: sequential model, The DenseNet-121, and ResNet-50. The accuracy, precision, and recall comparison of CNN models is displayed in table 3. Using the HAM10000 dataset, every model provides accuracy greater than 80%.

Table 3 presents a comparative analysis of CNN models. It reveals that the suggested CNN model, which employs a sequential method, has significantly higher accuracy than both other two methods. Additionally, layer optimization is employed to further enhance the accuracy of the proposed model. The training accuracy of the DenseNet121 is 89%, %, while the ResNet50-based model's validation accuracy is

84%. The validation accuracy of the sequential model is 98%. The sequential CNN model has 99% precision and recall, which is significantly greater than the other two models.

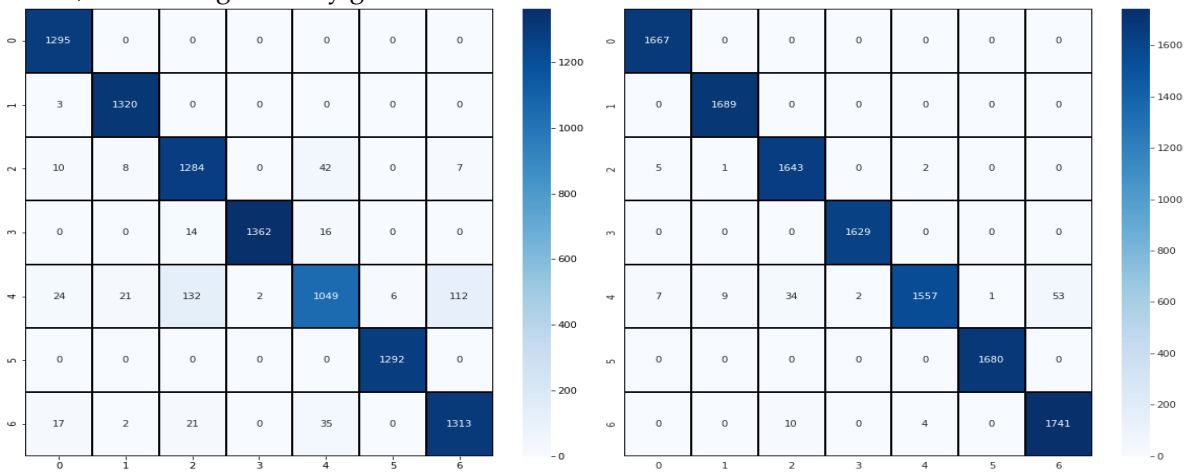

Figure 21. Confusion matrix

Table 3. Comparison of different CNN models

Model	Avg F1-score	Precision	Recall	Accuracy
DenseNet121	72%	69%	77%	89%
ResNet-50	68%	63%	78%	84%
Sequential CNN	99%	99%	99%	98%

5. Conclusion and Future Work

The basic objective of this research is the identification of skin diseases utilizing various deep learning-based models, including the Sequential CNN model, DenseNet-121, and ResNet-50. Our study's main goal is to construct and train a model using the ISIC archive's HAM10000 dataset. The model is based on a sequential CNN approach and has seven convolution layers for efficient batch normalization. The provided dataset is split into sets for training and testing, with an 80% and 20% ratio in each case. The dataset is expanded to lessen class imbalance and stop the model from overfitting, On the training dataset, the ResNet-50 model's accuracy is 91%, whereas on the testing dataset, it is 84%. DenseNet-121 achieved 93% accuracy on the training data set and 89% accuracy on the test data set. Using the HAM10000 dataset, the model built using sequential CNN technology and seven convolutional layers had 100% training accuracy and 98% validation or testing accuracy. The AUC values of the ROC curve of the proposed model for each skin disease category in the dataset is greater than 99%. The model's prediction accuracy is higher when it came to the dermatology category, which had more samples than other categories. The study uses several performance metrics to evaluate the effectiveness of the proposed model. The goal of the project is to enhance current methods for diagnosing skin conditions. In the future, skin disease diagnosis systems might have a framework in which a dermatologist cross-verifies the report produced by the model after it has identified the type of skin disease. The dermatologist may utilize their expertise to improve the model's prediction accuracy and suggest a course of action for the disease of the skin.

Author Contribution: Muddasar Abbas, Muhammad Arslan, Rizwan Abid Bhatty, Fatima Yousaf, Ammar Ahmad Khan, and Abdul Rafay conceptualized the methodology. Rizwan Bhatty helped implement deep learning models, particularly convolutional neural networks (CNNs), for diagnosing skin diseases using image data and data augmentation techniques to enhance accuracy. All authors contributed equally to the manuscript.

References

1. A. Magdy, H. Hussein, R. F. Abdel-Kader, and K. A. El Salam, "Performance Enhancement of Skin Cancer Classification Using Computer Vision," IEEE Access, vol. 11, pp. 72120–72133, 2023, doi: 10.1109/ACCESS.2023.3294974.
2. X. Xiao et al., "The role of short-chain fatty acids in inflammatory skin diseases," Front. Microbiol., vol. 13, p. 1083432, Feb. 2023, doi: 10.3389/FMICB.2022.1083432/BIBTEX.
3. M. Akrout et al., "Diffusion-Based Data Augmentation for Skin Disease Classification: Impact Across Original Medical Datasets to Fully Synthetic Images," Lect. Notes Comput. Sci. (including Subser. Lect. Notes Artif. Intell. Lect. Notes Bioinformatics), vol. 14533 LNCS, pp. 99–109, 2024, doi: 10.1007/978-3-031-53767-7_10.
4. M. A. Ilișanu, F. Moldoveanu, and A. Moldoveanu, "Multispectral Imaging for Skin Diseases Assessment—State of the Art and Perspectives," Sensors 2023, Vol. 23, Page 3888, vol. 23, no. 8, p. 3888, Apr. 2023, doi: 10.3390/S23083888.
5. B. Datten et al., "An Extensive Examination of the Warning Signs, Symptoms, Diagnosis, Available Therapies, and Prognosis for Lumpy Skin Disease," Viruses 2023, Vol. 15, Page 604, vol. 15, no. 3, p. 604, Feb. 2023, doi: 10.3390/V15030604.
6. M. Sharafudeen and V. C. S. S, "Detecting skin lesions fusing handcrafted features in image network ensembles," Multimed. Tools Appl., vol. 82, no. 2, pp. 3155–3175, Jan. 2023, doi: 10.1007/S11042-022-13046-0/TABLES/7.
7. H. Azgomi, F. R. Haredasht, and M. R. Safari Motlagh, "Diagnosis of some apple fruit diseases by using image processing and artificial neural network," Food Control, vol. 145, p. 109484, Mar. 2023, doi: 10.1016/J.FOODCONT.2022.109484.
8. D. A. Reddy, S. Roy, S. Kumar, and R. Tripathi, "Enhanced U-Net segmentation with ensemble convolutional neural network for automated skin disease classification," Knowl. Inf. Syst., vol. 65, no. 10, pp. 4111–4156, Oct. 2023, doi: 10.1007/S10115-023-01865-Y/TABLES/12.
9. T. Liu et al., "An expert knowledge-empowered CNN approach for welding radiographic image recognition," Adv. Eng. Informatics, vol. 56, p. 101963, Apr. 2023, doi: 10.1016/J.AEI.2023.101963.
10. Ambuj and R. Machavaram, "Neuromorphic computing spiking neural network edge detection model for content based image retrieval," Netw. Comput. Neural Syst., May 2024, doi: 10.1080/0954898X.2024.2348018.
11. A. Naeem, T. Anees, K. T. Ahmed, R. A. Naqvi, S. Ahmad, and T. Whangbo, "Deep learned vectors' formation using auto-correlation, scaling, and derivations with CNN for complex and huge image retrieval," Complex Intell. Syst., vol. 9, no. 2, pp. 1729–1751, Apr. 2023, doi: 10.1007/S40747-022-00866-8/FIGURES/20.
12. S. Devulapalli, A. Potti, R. Krishnan, and M. S. Khan, "Experimental evaluation of unsupervised image retrieval application using hybrid feature extraction by integrating deep learning and handcrafted techniques," Mater. Today Proc., vol. 81, no. 2, pp. 983–988, Jan. 2023, doi: 10.1016/J.MATPR.2021.04.326.
13. H. Rastegar and D. Giveki, "Designing a new deep convolutional neural network for content-based image retrieval with relevance feedback," Comput. Electr. Eng., vol. 106, p. 108593, Mar. 2023, doi: 10.1016/J.COMPELECENG.2023.108593.
14. M. A. Khan, K. Muhammad, M. Sharif, T. Akram, and S. Kadry, "Intelligent fusion-assisted skin lesion localization and classification for smart healthcare," Neural Comput. Appl., vol. 36, no. 1, pp. 37–52, Jan. 2024, doi: 10.1007/S00521-021-06490-W/FIGURES/10.
15. P. Kaushik, R. Rathore, A. Kumar, Kanishka, G. Goshi, and P. Sharma, "Identifying Melanoma Skin Disease Using Convolutional Neural Network DenseNet-121," 2024 IEEE Int. Conf. Interdiscip. Approaches Technol. Manag. Soc. Innov. IATMSI 2024, 2024, doi: 10.1109/IATMSI60426.2024.10502880.
16. A. Karambele, M. Tamhane, P. Jayanty, R. Patil, and K. Shirsat, "eDermaCare: Enhancing Skin Disease Classification with ResNet50," Proc. 18th INDIAcom; 2024 11th Int. Conf. Comput. Sustain. Glob. Dev. INDIACom 2024, pp. 1008–1014, 2024, doi: 10.23919/INDIACOM61295.2024.10499009.
17. R. Sadik, A. Majumder, A. A. Biswas, B. Ahammad, and M. M. Rahman, "An in-depth analysis of Convolutional Neural Network architectures with transfer learning for skin disease diagnosis," Healthc. Anal., vol. 3, p. 100143, Nov. 2023, doi: 10.1016/J.HEALTH.2023.100143.
18. S. Shivadekar, B. Kataria, S. Limkar, K. S.Wagh, S. Lavate, and R. A. Mulla, "Design of an efficient multimodal engine for preemption and post-treatment recommendations for skin diseases via a deep learning-based hybrid bioinspired process," Soft Comput., pp. 1–19, Jun. 2023, doi: 10.1007/S00500-023-08709-5/FIGURES/11.
19. Y. Yanagisawa, K. Shido, K. Kojima, and K. Yamasaki, "Convolutional neural network-based skin image segmentation model to improve classification of skin diseases in conventional and non-standardized picture images," J. Dermatol. Sci., vol. 109, no. 1, pp. 30–36, Jan. 2023, doi: 10.1016/J.JDERMSCI.2023.01.005.
20. K. V. Swamy and B. Divya, "Skin Disease Classification using Machine Learning Algorithms," Proc. 2021 2nd Int. Conf. Commun. Comput. Ind. 4.0, C2I4 2021, 2021, doi: 10.1109/C2I454156.2021.9689338.
21. G. Cai, Y. Zhu, Y. Wu, X. Jiang, J. Ye, and D. Yang, "A multimodal transformer to fuse images and metadata for skin disease classification," Vis. Comput., vol. 39, no. 7, pp. 2781–2793, Jul. 2023, doi: 10.1007/S00371-022-02492-4/TABLES/6.
22. P. V. S. P. Raghavendra, C. Charitha, K. G. Begum, and V. B. S. Prasath, "Deep Learning–Based Skin Lesion Multi-class Classification with Global Average Pooling Improvement," J. Digit. Imaging, vol. 36, no. 5, pp. 2227–2248, Oct. 2023, doi: 10.1007/S10278-023-00862-5/TABLES/10.
23. A. Parashar, A. Parashar, W. Ding, M. Shabaz, and I. Rida, "Data preprocessing and feature selection techniques in gait recognition: A comparative study of machine learning and deep learning approaches," Pattern Recognit. Lett., vol. 172, pp. 65–73, Aug. 2023, doi: 10.1016/J.PATREC.2023.05.021.
24. O. Jaiyeoba, E. Ogbuju, O. T. Yomi, and F. Oladipo, "Development of a Model to Classify Skin Diseases using Stacking Ensemble Machine Learning Techniques," J. Comput. Theor. Appl., vol. 2, no. 1, pp. 22–38, May 2024, doi: 10.62411/JCTA.10488.

25. K. V. Swamy, V. Radhika, and R. D. Kadiyala, "Skin Disease Classification using Image Preprocessing and Machine Learning," 2024 IEEE Int. Conf. Interdiscip. Approaches Technol. Manag. Soc. Innov. IATMSI 2024, 2024, doi: 10.1109/IATMSI60426.2024.10502445.
26. A. De, N. Mishra, and H. T. Chang, "An approach to the dermatological classification of histopathological skin images using a hybridized CNN-DenseNet model," PeerJ Comput. Sci., vol. 10, p. e1884, Feb. 2024, doi: 10.7717/PEERJ-CS.1884.
27. L. Huang, J. Qin, Y. Zhou, F. Zhu, L. Liu, and L. Shao, "Normalization Techniques in Training DNNs: Methodology, Analysis and Application," IEEE Trans. Pattern Anal. Mach. Intell., vol. 45, no. 8, pp. 10173–10196, Aug. 2023, doi: 10.1109/TPAMI.2023.3250241.
28. H. Singh, A. S. Ahmed, F. Melandsø, and A. Habib, "Ultrasonic image denoising using machine learning in point contact excitation and detection method," Ultrasonics, vol. 127, p. 106834, Jan. 2023, doi: 10.1016/J.ULTRAS.2022.106834.
29. F. Bozkurt, "Skin lesion classification on dermatoscopic images using effective data augmentation and pre-trained deep learning approach," Multimed. Tools Appl., vol. 82, no. 12, pp. 18985–19003, May 2023, doi: 10.1007/S11042-022-14095-1/TABLES/9.
30. M. Wei et al., "A Skin Disease Classification Model Based on DenseNet and ConvNeXt Fusion," Electron. 2023, Vol. 12, Page 438, vol. 12, no. 2, p. 438, Jan. 2023, doi: 10.3390/ELECTRONICS12020438.
31. S. Lu, Y. Ding, M. Liu, Z. Yin, L. Yin, and W. Zheng, "Multiscale Feature Extraction and Fusion of Image and Text in VQA," Int. J. Comput. Intell. Syst., vol. 16, no. 1, pp. 1–11, Dec. 2023, doi: 10.1007/S44196-023-00233-6/TABLES/4.
32. Z. Wang, Z. Wang, C. Zeng, Y. Yu, and X. Wan, "High-Quality Image Compressed Sensing and Reconstruction with Multi-scale Dilated Convolutional Neural Network," Circuits, Syst. Signal Process., vol. 42, no. 3, pp. 1593–1616, Mar. 2023, doi: 10.1007/S00034-022-02181-6/FIGURES/8.
33. S. U. Rahman, F. Alam, N. Ahmad, and S. Arshad, "Image processing based system for the detection, identification and treatment of tomato leaf diseases.," Multimed. Tools Appl., vol. 82, no. 6, pp. 9431–9445, Mar. 2023, doi: 10.1007/S11042-022-13715-0/TABLES/5.
34. C. Dewi, R. C. Chen, Y. C. Zhuang, X. Jiang, and H. Yu, "Recognizing Road Surface Traffic Signs Based on Yolo Models Considering Image Flips," Big Data Cogn. Comput. 2023, Vol. 7, Page 54, vol. 7, no. 1, p. 54, Mar. 2023, doi: 10.3390/BDCC7010054.
35. F. Alrasheedi, X. Zhong, and P. C. Huang, "Padding Module: Learning the Padding in Deep Neural Networks," IEEE Access, vol. 11, pp. 7348–7357, 2023, doi: 10.1109/ACCESS.2023.3238315.
36. S. Mei, R. Jiang, M. Ma, and C. Song, "Rotation-Invariant Feature Learning via Convolutional Neural Network With Cyclic Polar Coordinates Convolutional Layer," IEEE Trans. Geosci. Remote Sens., vol. 61, 2023, doi: 10.1109/TGRS.2022.3233726.
37. C. Palai, P. Kumar Jena, S. Ranjan Pattanaik, T. Panigrahi, and T. Kumar Mishra, "Content-based Image Retrieval using Encoder based RGB and Texture Feature Fusion," IJACSA) Int. J. Adv. Comput. Sci. Appl., vol. 14, no. 3, p. 2023, Accessed: May 14, 2024. [Online]. Available: www.ijacsa.thesai.org
38. K. Lin, H. F. Yang, J. H. Hsiao, and C. S. Chen, "Deep learning of binary hash codes for fast image retrieval," IEEE Comput. Soc. Conf. Comput. Vis. Pattern Recognit. Work., vol. 2015-Octob, pp. 27–35, 2015, doi: 10.1109/CVPRW.2015.7301269.
39. F. Alenezi, A. Armghan, and K. Polat, "Wavelet transform based deep residual neural network and ReLU based Extreme Learning Machine for skin lesion classification," Expert Syst. Appl., vol. 213, p. 119064, Mar. 2023, doi: 10.1016/J.ESWA.2022.119064.
40. A. N. Holm, D. Wright, and I. Augenstein, "Revisiting Softmax for Uncertainty Approximation in Text Classification," Inf. 2023, Vol. 14, Page 420, vol. 14, no. 7, p. 420, Jul. 2023, doi: 10.3390/INFO14070420.
41. T. X. Truong et al., "A New Approach Based on TensorFlow Deep Neural Networks with ADAM Optimizer and GIS for Spatial Prediction of Forest Fire Danger in Tropical Areas," Remote Sens. 2023, Vol. 15, Page 3458, vol. 15, no. 14, p. 3458, Jul. 2023, doi: 10.3390/RS15143458.
42. J. Li, H. Sun, and J. Li, "Beyond confusion matrix: learning from multiple annotators with awareness of instance features," Mach. Learn., vol. 112, no. 3, pp. 1053–1075, Mar. 2023, doi: 10.1007/S10994-022-06211-X/TABLES/4.
43. D. Krstinic, L. Seric, and I. Slapnicar, "Comments on 'MLCM: Multi-Label Confusion Matrix,'" IEEE Access, 2023, doi: 10.1109/ACCESS.2023.3267672.
44. F. Wu et al., "Detection and counting of banana bunches by integrating deep learning and classic image-processing algorithms," Comput. Electron. Agric., vol. 209, p. 107827, Jun. 2023, doi: 10.1016/J.COMPAG.2023.107827.
45. J. N. Saeed, A. M. Abdulazeez, and D. A. Ibrahim, "Automatic Facial Aesthetic Prediction Based on Deep Learning with Loss Ensembles," Appl. Sci. 2023, Vol. 13, Page 9728, vol. 13, no. 17, p. 9728, Aug. 2023, doi: 10.3390/APP13179728.
46. S. Kumar, A. K. Pal, S. H. Islam, and M. Hammoudeh, "Secure and efficient image retrieval through invariant features selection in insecure cloud environments," Neural Comput. Appl., vol. 35, no. 7, pp. 4855–4880, Mar. 2023, doi: 10.1007/S00521-021-06054-Y/FIGURES/22.
47. E. S. Sabry et al., "Image Retrieval Using Convolutional Autoencoder, InfoGAN, and Vision Transformer Unsupervised Models," IEEE Access, vol. 11, pp. 20445–20477, 2023, doi: 10.1109/ACCESS.2023.3241858.
48. M. A. Aboali, I. Elmaddah, and H. E. Abdelmunim, "Neural Textual Features Composition for CBIR," IEEE Access, vol. 11, pp. 28506–28521, 2023, doi: 10.1109/ACCESS.2023.3259737.